Hindawi Publishing Corporation
Advances in Meteorology
Volume 2014, Article ID 960924, 15 pages
http://dx.doi.org/10.1155/2014/960924

Research Article

A Numerical Investigation of the Precipitation over Lake Victoria Basin Using a Coupled Atmosphere-Lake Limited-Area Model

Xia Sun, Lian Xie, Fredrick H. M. Semazzi, and Bin Liu

Department of Marine, Earth and Atmospheric Sciences, North Carolina State University, Raleigh, NC 27695, USA

Correspondence should be addressed to Bin Liu; bliu5@ncsu.edu

Received 18 May 2014; Revised 5 August 2014; Accepted 6 August 2014; Published 15 September 2014

Academic Editor: Richard Anyah

By using a coupled atmosphere-lake model, which consists of the Weather Research and Forecasting (WRF) model and the Princeton Ocean Model (POM), the present study generated realistic lake surface temperature (LST) over Lake Victoria and revealed the prime importance of LST on the precipitation pattern over the Lake Victoria Basin (LVB). A suite of sensitivity experiments was conducted for the selection of an optimal combination of physics options including cumulus, microphysics, and planetary boundary layer schemes for simulating precipitation over the LVB. The WRF-POM coupled system made a great performance on simulating the expected LST, which is featured with eastward temperature gradient as in the real bathymetry of the lake. Under thorough examination of diagnostic analysis, a distinguished diurnal phenomenon has been unveiled. The precipitation mainly occurs during the nocturnal peak between midnight and early in the morning, which is associated with the strong land breeze circulation, when the lake temperature is warmer than the adjacent land. Further exploration of vertical velocity, surface divergence pattern, and maximum radar reflectivity confirms such conjecture. The time-longitude analysis of maximum radar reflectivity over the entire lake also shows a noticeable pattern of dominating westward propagation.

1. Introduction

Lake Victoria, along with Lake Tanganyika and Lake Malawi, located in Eastern Africa, together form a favorable environment for the interactions between local and large-scale circulations. Lake Victoria is the largest tropical lake in the world and economically supports over sixty million inhabitants over surrounding areas. The lake is affected by several dominant seasonal and interannual factors, such as Intertropical Convergence Zone (ITCZ), El Nino/Southern Oscillation (ENSO), complex orographic forcing, and anomaly Indian Ocean zonal temperature gradient.

The atmosphere and its underlying water bodies (including oceans and lakes) constitute an intimately coupled system on the Earth. The two components are complexly linked to each other and are responsible for Earth's weather and climate. The pioneer attempts of coupling the atmospheric and oceanic models can be traced back to the late 1960s and early 1970s [1–3]. Since then, coupled atmosphere-ocean (or lake) models have been continuously modified and improved in order to understand and predict climatic variability and climate change.

Song et al. [4] employed a fully coupled threedimensional atmospheric-lake modeling system, which consists of the second-generation regional climate modeling system (RegCM2) and the lake version of the Princeton Ocean Model (POM), to explore the catchment-scale and regional climate around the Lake Victoria Basin (LVB). They abandoned the traditional modeling approach that neglects the importance of hydrodynamics and bases the formulation entirely on the thermodynamics alone; however, taking both hydrodynamics and thermodynamics into account, brought

satisfactory results when applyied to the LVB. And through the coupled process, the lake surface temperature (LST) field was successfully produced with an eastward gradient pattern, in which warmer water is located over the shallower region of the western sector of the lake, while colder water is contained in the relatively deeper eastern part. Besides, the asymmetric LST pattern impacts the overlying wind field and, in turn, modifies the cloud cover and overlake rainfall intensity. In the subsequentyears, RegCM3, which is an improved and augmented version of RegCM2, was adopted and coupled to the POM, an oceanic model, developed by Anyah [5] in order to further study the features and physical mechanisms associated with Lake Victoria's climatic variability. In particular, the significant influence of large-scale transported moisture via the lateral boundary was verified on the remarkable enhancement/suppression of simulated rainfall over the targeted lake region. In addition, there are also studies [6, 7] introducing other lake models in applications of nearby tropical lakes. Thiery and coauthors [7] presented the results of the Lake Model Intercomparison Project (LakeMIP) for Lake Kivu, which involved seven one-dimensional lake models.

Recently, a fully coupled atmosphere-wave-ocean modeling system (CAWOMS) was established by a series of studies [8–10]. The CAWOMS consists of a new-generation atmospheric model, the Weather Research and Forecasting (WRF) model, an oceanic circulation model, the POM model, and a third generation wave model, called the Simulating Waves Nearshore (SWAN) model. The CAWOMS has been applied to several tropical cyclone studies in order to investigate the impact of atmosphere-wave-ocean interaction and coupling on tropical cyclone systems. In this study, we aim to establish an atmosphere-lake coupled model for the LVB by modifying the atmosphere-ocean coupling component of the CAWOMS and then demonstrate its capability in producing realistic lake surface temperature (LST), thus resulting in better simulation of precipitation over the LVB. Through a series of sensitivity simulations of the precipitation over the LVB, it has been demonstrated that the LST has a detrimental impact on the rainfall over the LVB [11]. However, given the failure of existing global models in providing realistic LSTs for the LVB, while also considering the lack of lake observational data over this region, the coupled atmosphere-lake model, which takes into account the air-lake interaction processes, is expected to obtain a realistic lake circulation including its LST pattern. Besides, one of the merits of this study is coupling a three-dimensional (3-D) lake model modified from the POM ocean model to a state-of-the-art regional atmospheric model, the WRF model.

The rest of this study is organized into the following sections. Detailed description of the three-dimensional fully coupled atmosphere-lake model will be introduced in Section 2, along with the model settings and experimental design. Analyses of the simulation results of overlake precipitation under various LST patterns over Lake Victoria will be briefly reviewed in Section 3, together with the findings and examinations about rainfall simulation with the coupled model. Section 4 will present the summary and conclusions.

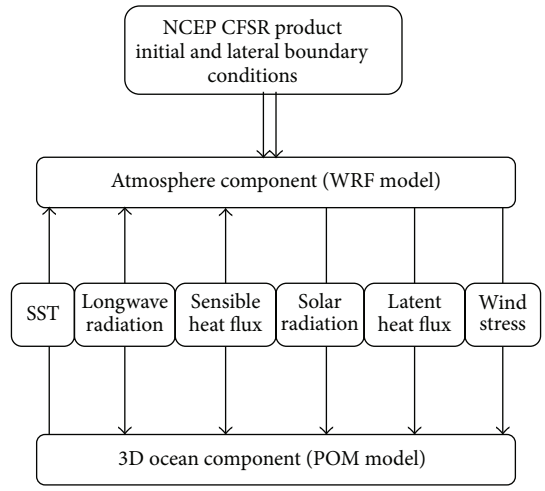

Figure 1: The schematic illustration of the coupled atmosphere-lake system.

2. The Coupled Atmosphere-Lake Model and Experimental Design

2.1. Description of Coupled Atmosphere-Lake Model. The coupled atmosphere-lake model is constructed based on the atmosphere-ocean coupling system of the CAWOMS, which is a fully coupled atmosphere-wave-ocean model developed by Xie et al. [8], Liu et al. [9], and Liu et al. [10]. It consists of an atmospheric regional version of the Weather Research and Forecasting (WRF) model, Version 3.2 [12], and the Princeton Ocean Model (POM) [13], which is an ocean circulation model. The POM model is configured to conduct lake circulation simulation. The model components are connected to each other through the Model Coupling Toolkit [14, 15] which is a set of open source software tools written by Fortran90 and works with Message Passing Interface (MPI) communication protocol. It was previously employed as the basis for the Community Climate System Model coupler [16] as well as the Regional Ocean Modeling System [17].

Figure 1 illustrates the interaction within the coupled atmosphere-lake model. The procedure generally depicts that the atmospheric model component drives the lake circulation model component through various atmospheric forcings including surface wind stress, longwave and shortwave radiation, latent and sensible heat flux, and atmospheric sea level pressure. In turn, the lake circulation model component provides time-dependent LST to the atmospheric model component to calculate heat fluxes at the air-lake interface. Moreover, the lake circulation model component contributes to the lake surface current in order to estimate the relative wind speed for the computation of surface wind stress. Variables are exchanged between two model components at certain time intervals determined beforehand.

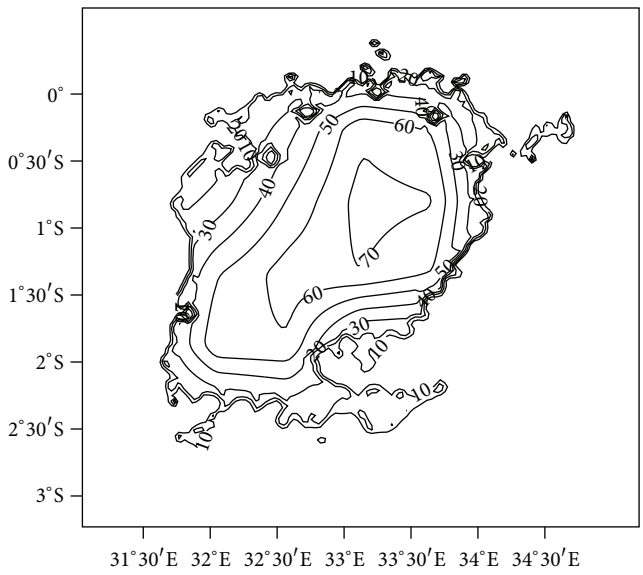

Figure 2: The bathymetry of Lake Victoria.

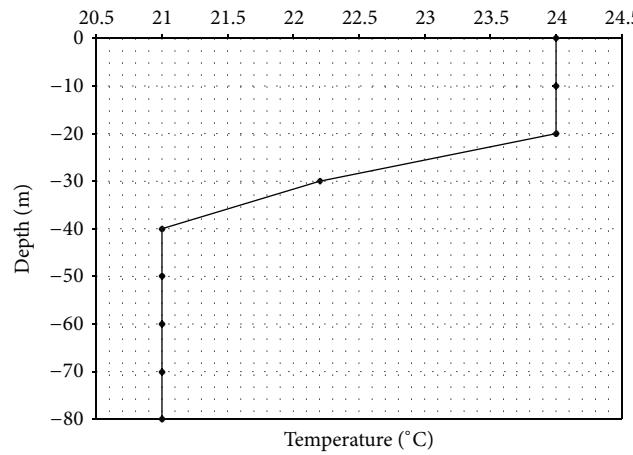

Figure 3: Initial vertical temperature profile for Lake Victoria.

More detailed information about the model components, coupled procedure, and the parameterization of atmosphere-lake interaction processes are referred to in Liu et al. [9].

There are several simplifications that need to be taken into consideration in terms of applying the coupled model to the Lake Victoria basin. Given the fact that the main striking feature making freshwater lakes distinguished from coastal ocean is the salinity effects, salinity for the lake circulation model component in this study is set to a constant value of 0.2 PSU, which has been examined as a suitable estimate [18] when applying POM to the simulations of the Lake Victoria region. Also, tides are not taken into consideration for the lake model. In addition, the lake model domain is completely enclosed by the land so that the open boundary conditions are ruled out. We also neglect the effects of evaporation, precipitation, and river runoff on the elevation of the lake, which is supported by the diagnostic analysis conducted by Yin and Nicholson [19]. They confirmed that the river inflow and discharge are relatively much smaller than the contributions of evaporation and rainfall in the hydrological budget of Lake Victoria. The real bathymetry (Figure 2) of Lake Victoria is employed, which has a significantly steeper coastal vertical slope on the eastern side of the lake than that on the western side. The maximum depth of the lake is 74 m, and the minimum depth for the lake model component is set to 10 m. The initial temperature vertical profile is shown in Figure 3. The climatological surface temperature of 24°C is prescribed for the upper 20 m of the lake, and then the temperature decreases gradually with depth for the following 20 m layer until it reaches the isothermal condition, once again, where it maintains the same constant temperature value all the way down to the bottom of the boundary layer. The temperature profile adopted here is consistent with the one in Anyah [5].

2.2. Design of Numerical Experiments. The response of precipitation distribution to the change of LST was investigated in a previous study [11], in which the first-order role of LST was isolated and demonstrated to have a critical influence on precipitation over the LVB through various sensitivity simulations. However, due to the relatively coarse resolution of the global model, which has difficulty resolving the lake and the relatively poor observation system over the LVB, a relatively realistic LST pattern over LVB is currently not available from global models. Failure to provide a realistic LST pattern over LVB will thus lead to unfavorable simulation of the precipitation pattern. Therefore, we employed the coupled atmospheric-lake model with sufficient spin-up processes in advance and real-time exchanges of different atmospheric forcings to generate lake temperature structure and circulation fields of Lake Victoria. Once the expected LST pattern was reproduced by using the coupled atmosphere-lake system, diurnal features were thereupon examined and analyzed based on the simulation results.

All the simulations conducted in this study are during the short rainy season of Eastern Africa, in 1999, which is a normal or neutral climate year, meaning that there is neither a La Nina nor an El Nino happening. Furthermore, in accordance with previous LST sensitivity experiments in Sun et al. [11], the exploration of the LST pattern and subsequent analyses are focused on a five-day short case as well. The model domains for the atmospheric model component include a nested 4 km spatial resolution grid within a 12 km grid. The inner domain is approximately centered at 33°E, 1.4°S, and the whole lake is covered by the 121 × 121 grid meshes. The model domains are on the Mercator map projection and have 30 vertical levels with the top of the atmosphere placed at 50 hPa. The time step is fixed at 60 seconds for the parent domain and model outputs are archived every 3 hours during the simulation period. The physical schemes including Eta microphysics [20], improved Grell-3D cumulus [21], and ACM2 planetary boundary layer scheme [22, 23], along with MM5 similarity surface layer scheme [24] and Noah land surface model [25] are selected based on previous sensitivity simulations [26, 27]

and experiments described as follows. Correspondingly, the lake circulation model component uses the same horizontal grid meshes as the nested 4 km atmospheric inner model domain. POM model consists of 12 sigma vertical layers and the external and internal time steps are 15 and 450 seconds, respectively.

The lake circulation model component was first integrated 60 days independently using the 6-hourly NCEP Reanalysis data for model spin-up, during which, time-dependent forcings from October to November of 1999 were adopted to drive the lake circulation model. Considering the lake's depth and large surface area, such a long time is helpful for the lake to respond well to the atmospheric forcings. Since the large-scale prevailing flow over Eastern Africa is dominated by the easterly trade winds most of the year, the surface wind stress was fixed as a constant easterly flow during the simulation period. Thereafter, the results from the oceanic spin-up process were used as the initial conditions for the POM component in the two-month coupled process. On the other hand, NCEP Climate Forecast System Reanalysis (CFSR) data, which consists of higher spatial resolution and superior quality, provided the initial and boundary conditions for the stand-alone atmospheric model component. Since the target is to produce realistic lake temperature patterns, the model coupling is currently configured for the model domain with a 4 km grid resolution. The outputs of the outer atmospheric model with coarser-grid resolutions were used to generate the initial and boundary conditions for the inner 4 km atmospheric model domain. And eventually, the generated LST pattern from the coupled model was reinterpolated into the outer coarse atmospheric model domain to replace the original LST, in order to accomplish the five-day simulation and avoid inconsistency in the physics and dynamics of the two atmospheric model domains. As mentioned above, we still chose the same five-day time period as an extension of our previous study and also to testify that a proper description of LST would really help to improve the simulation of precipitation and that the coupled system is a feasible way to employ in the further studies over the LVB region.

3. Results and Discussions

3.1. Sensitivity Experiments for the Physics Options of the Atmospheric Model. Davis et al. [28] presented a particular view of customizing the rainfall processes over the tropical regions of eastern Africa and the Indian Ocean using the RegCM3 model. Since precipitation has been such an important research topic in many areas throughout the world, proper customization and representation of its amount and distribution would be of the utmost importance before further exploring the related processes and predicting the variability. Therefore, sensitivity experiments were first conducted to determine the optimal settings of the physics options of the WRF model in simulating the precipitation over the LVB. Among all the available physics options, we selected and compared the planetary boundary layer, microphysics, and cumulus schemes in terms of their critical

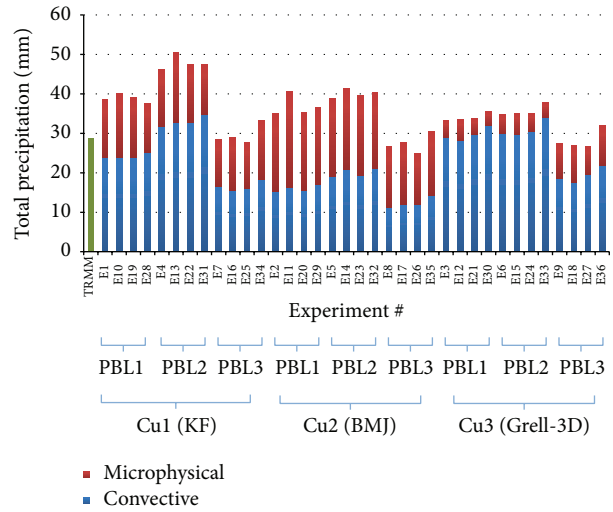

Figure 4: The area-averaged microphysical (red) and cumulus (blue) rainfall over the entire nested domain from 36 combinations of physical parameterization schemes together with the TRMM data (green).

effects on the formation of model precipitation. The cumulus scheme is primary in a way that it exerts an influence on producing the convective rainfall, which dominates over the tropical regions [29, 30]. The choice of the planetary boundary layer (PBL) scheme will directly affect the temperature and moisture profile in the lower troposphere and the turbulent mixing of all levels as well, which can pull the trigger on convective activity. In addition, the microphysics scheme is responsible for heat exchanges taking place inside the clouds and indirectly influencing the radiation budget at the surface and at the top of the atmosphere [31, 32]. A suite of 36 simulations was executed for the five-day case, corresponding to all the possible combinations among four microphysics, three PBL, and three cumulus schemes. Table 1 summarizes the selected schemes and their main characteristics. They all share the same parameters of other physical schemes, including the shortwave and longwave parameterization schemes by Dudhia [33] and Mlawer (RRTM, [34]), respectively, and Noah Land Surface Model [25] for the land surface scheme. The land use was prescribed by a set of land-surface categories provided by the Moderate Resolution Imaging Spectroradiometer (MODIS, 20 classes: [35]). The simulated rainfall was compared to the interpolated TRMM data with the main focus being over the lake region during five-day period.

In general, different physical options generate rainfall with varied intensities and patterns in both the parent and nesting domains. Figure 4 provides the area-averaged five-day total rainfall and separate cumulus and microphysical rainfall over the entire nesting domain from each simulation compared with observational data. Every four simulations share the same PBL scheme in Figure 4, with the microphysics schemes in sequence using WSM6, Morrison, Lin, and Eta. The MP and PBL physical schemes appear to exert relatively less influence than the Cu scheme on the produced rainfall

Table 1: Summary of cumulus, planetary boundary layer, and microphysics parameterization schemes used in this study.

(a) Cumulus schemes

KF: Kain-Fritsch scheme	BMJ: Betts-Miller-Janjic scheme	Grell-3D: Improved Grell-Devenyi (GD) ensemble scheme
Low-level control convective scheme and entraining-detraining mass flux scheme	Convective adjustment scheme: instability is eliminated by nudging environmental profiles of temperature and specific humidity empirically derived reference profiles	An improved version of GD scheme that may also be used on high resolution if subsidence spreading is turned on

(b) Planetary boundary layer schemes

YSU: Yonsei University scheme	MYJ/TKE: Mellor-Yamada-Janjic scheme	ACM2: Asymmetric Convective Model version 2
First-order nonlocal scheme	2.5 turbulent closure modified Mellor and Yamada scheme based on Turbulent Kinetic Energy (TKE)	Nonlocal closure scheme with eddy diffusion

(c) Microphysics schemes

WSM6: WRF Single-Moment 6-class scheme	Morrison: Morrison double-moment scheme	Lin: Lin et al. scheme	Eta: Eta microphysics for fine resolution
Extension of the WSM5 scheme including graupel and associated processes	Scheme including vapor, cloud droplets, cloud ice, rain, snow, and graupel/hail. Prediction of two-moment (number of concentration and mixing ratio) allowing for a more robust treatment of the particle size distributions	Hydrometeors including water vapor, cloud water, rain, cloud ice, snow, and graupel and scheme is taken from Purdue cloud model and details can be found in [37]	Operational scheme in NCEP models with diagnostic mixed-phase processes

intensity. As a consequence, computed statistical errors over the nesting region mainly vary according to the Cu scheme, with lower (higher) values being found with the Grell-3D (KF) scheme. The microphysics scheme seems to exert slight, but still not negligible, influence on the short-term rainfall, unlike the little impact from the PBL schemes. Experiments with Eta and WSM6 MP schemes generate the least rainfall bias against satellite observed rainfall data. To be more specific, the Grell-3D scheme contributes to more of the convective precipitation, given its percentage in the total rainfall, while the KF and BMJ scheme evenly match one another. In addition, the effect of combinations between the convective and microphysics schemes is more or less additive; in other words, the largest rainfall amounts are obtained when the KF scheme is combined with the Morrison/Lin MP scheme, while the driest amounts are obtained when the Grell-3D scheme is combined with the WSM6/Eta scheme.

Each experiment produces various precipitation patterns which are not shown here. However, compared with the TRMM data, none of the simulations give the two-rainfall maxima, which are featured in the observation and all fail to capture the western rainfall maximum, which is up to 209.5 mm in the observation. Additionally, the precipitation is mainly concentrated over the adjacent land, especially over the eastern coastal areas. It is now the meaningful point where we realize the deficient capability of the regional model on simulating rainfall over the Lake Victoria basin and the point where we start to explore the underlying reasons. In spite of the very fact that Grell-3D makes a good performance in both domains, the impact of the domain size and lateral boundaries shows their importance with the domain center changing, as earlier studies suggested. As indicated by statistical analysis, WSM6 MP in combination with the MYJ PBL scheme works well for the parent domain, while Eta MP coupled with the ACM2 PBL scheme is associated with the least rainfall bias shown here, however, under insufficient amounts of rainfall.

To sum up, the comparisons of both the precipitation patterns and the intensity demonstrate that the combined use of the Eta microphysics scheme with an improved Grell-3D cumulus scheme as well as an Asymmetric Convective Model (ACM2) planetary boundary layer scheme, along with the MM5 similarity surface layer scheme, yields the most satisfactory distribution over the lake and adjoining land areas in the present study.

3.2. The Importance of LST on Rainfall over LVB. It is well known that the precipitation over Eastern Africa is strongly influenced by the progression of the ITCZ twice a year,

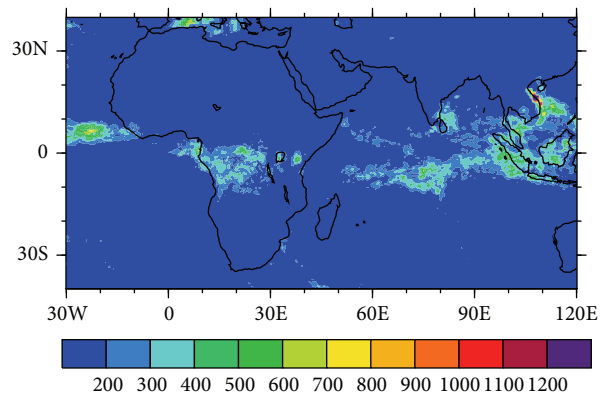

FIGURE 5: Rainfall (in mm) during November from the TRMM data.

leading to a remarkable bimodal rainfall feature. Figure 5 gives the total rainfall belt during the month of November of the simulation year from an observation that coincides with the annual mean location of the ITCZ over the areas of Africa and the Indian Ocean. In Sun et al. [11], a set of rainfall patterns under various LST forcings is presented in Figure 6. The comparisons between the top two figures show the incapability of the regional model, with insufficient LSTs, in producing the rainfall variability over the LVB once again. The control run clearly fails to simulate the remarkable two-rainfall maxima feature observed in the TRMM data. The rainfall is less intense under default settings, with an area-averaged temperature value being only 20°C. However, there is an apparent intensification/weakening of rainfall over and in the vicinity of the lake occurring with temperature being increased/decreased for the asymmetric LST distribution as shown in Figures 6(c), 6(d), and 6(e). It is worth noting that the relation between rainfall anomalies and the LST variations is nonlinear. When the lake is warmer by 1.5°C, there is only a slight increment and the two-rainfall maxima are starting to show. Nevertheless, it disappears with area-averaged temperature being 25.5°C and is replaced by a single rainfall concentration over the middle of the lake. We postulate that the primary physical mechanism switches from the temperature gradient-driven between the lake and land into the convection-driven over the lake. It seems that in the current case, the area-averaged temperature is maintained around 24°C and is the prerequisite for obtaining a better rainfall pattern.

Besides, we found that the bias in area-averaged LST from about 24°C is more detrimental for the simulation of rainfall over the lake basin than the sensitivity on the general LST distribution, although the latter is also important which is shown in Figure 6(f) case. We adopted the LST pattern from Anyah [5], which is characterized by the eastward temperature gradient as dictated by the lake bathymetry. The corresponding rainfall field showed the two-rainfall maxima pattern with the highest amount located over the western sector of the lake for the first time, which is the most consistent simulation with observation among all the experiments. We only care about the role of the LST in the overlake rainfall; however, there are other factors that might control the precipitation field as suggested by the ever-present rainfall concentration over the eastern sector of the lake, which will be discussed later.

3.3. Hydrodynamic Characteristics of Lake from Coupled Model. The basic wind structure associated with the LVB is predominated by the northeasterly monsoon flow during the North Hemisphere winter and the southeasterly flow during the North Hemisphere summer. Given the uncertainties of variable distribution of existing available datasets and inaccessibility of reliable gauge data, the stand-alone lake circulation model component is integrated by adopting a prescribed uniform surface temperature of 24°C and an idealized constant easterly flow along with CFSR time-dependent atmospheric forcings for the model spin-up. With the constraint of constant surface temperature, the lake stratification would become more stable with continuous mixing due to downwelling and upwelling. The surface water current after two-month integration is presented in Figure 7. The surface circulation is basically barotropic, where the Coriolis effect is nearly negligible. One small gyre circulation is formed centering in the middle of the lake. The mass continuity dynamic law indicates that upwelling is initiated along the eastern coastline and downwelling motion exists along the western boundary of the lake, resulting in divergence and convergence at the water surface, respectively.

Such a theory is again verified in the evolution of lake surface temperature pattern at the beginning of the coupling process. After 10 days of model integration (Figure 8(a)), the strong upwelling brings colder water from the bottom of the lake to the surface and results in a temperature decrease. In addition, intense upwelling occurs all across the eastern sector of the lake, with the maximum upwelling being located at the northeastern part of the lake. However, the surface temperature over the western sector is still as warm as the initial temperature setting, which is in good agreement with the downwelling motion underneath. The lake reaches equilibrium at around 40 days of simulation and starts to heat up over the whole lake. Figure 8(b) shows the lake surface temperature pattern after the two-month integration through the coupled model. The western part of the lake heats up much faster than the rest of the lake during the day, as dictated by the real bathymetry, with the shallower region located over the western sector of the lake. The area-averaged LST approaches 25.12°C. The eastward temperature gradient is well simulated with higher temperatures over the northwestern sector of the lake. The general structure of the lake temperature is in accordance with the LST pattern from Anyah [5], but is feeding with real-time dependent forcings from the regional atmospheric model. Consequently, compared with LST pattern under simple idealized easterly wind stress in their study, Figure 8(b) displays a more complex temperature distribution with a more intense temperature gradient concentrated over the western part of the lake and over the eastern cold tongue-extending into the middle of the lake.

3.4. Diagnostic Analysis of Diurnal Feature of Lake. We extracted the LST pattern shown in Figure 8(b) from the

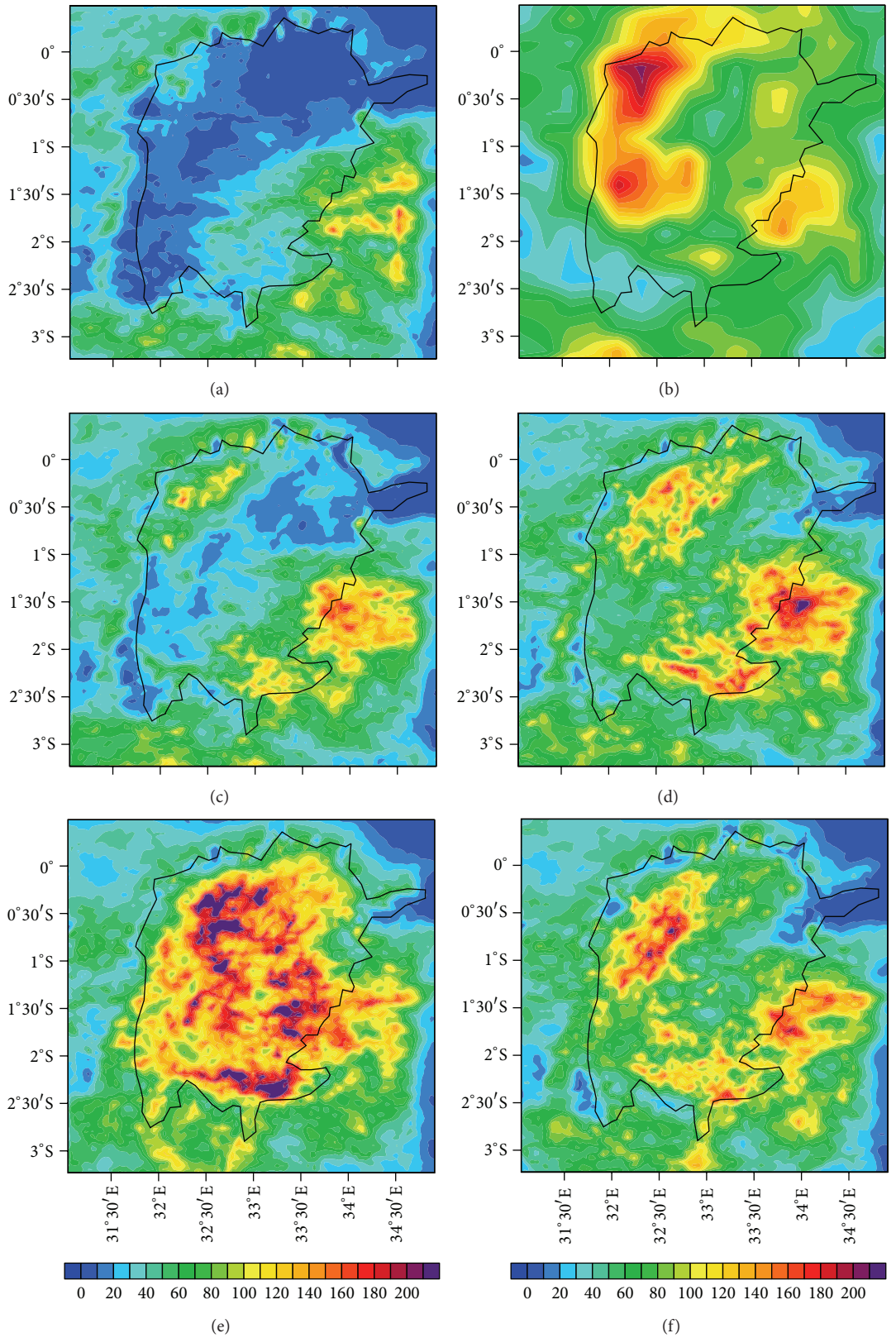

Figure 6: Total rainfall pattern during the five-day period from (a) the control run, (b) the TRMM data, (c, d, e) the experiments with area-averaged LST being 22.5°C, 24°C, and 25.5°C, and (f) the experiments with LST pattern from Anyah [5].

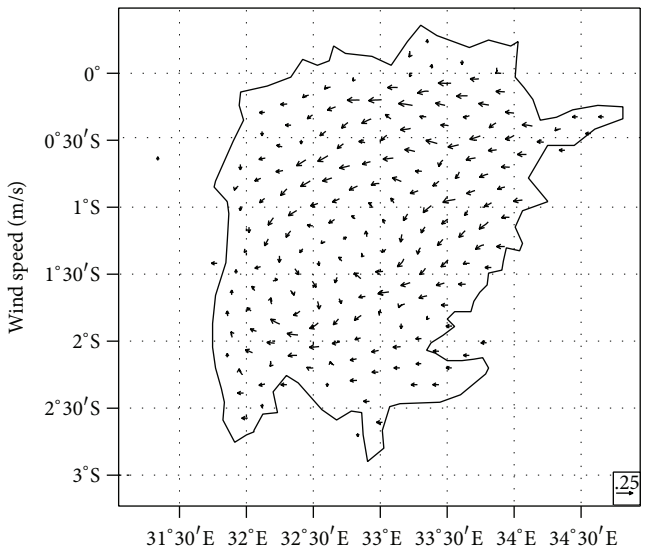

Figure 7: Simulated lake surface current (in m s^{-1}) after two-month integration under the forcing of uniform wind stress.

CFSR-coupled run and then fed it into the stand-alone atmospheric model to accomplish the five-day total precipitation simulation. One modification that needs to be emphatically pointed out is the fact that the adopted LSTs at every lake point were subtracted by 1°C so that the area-averaged value approached 24°C, which is the prerequisite in the current case study to generate a consistent rainfall pattern with observation from previous discussion. The total rainfall distribution is exhibited in Figure 9 compared with the observation. Apparently, the two-rainfall maxima pattern is successfully reproduced with the highest rainfall amount located over western sector of the lake. The maximum western and eastern precipitation amounts reach 219.4 mm and 205.3 mm, respectively. The rainfall is concentrated over the coastal regions and the exact locations of the two maxima are getting closer to the TRMM data with only being slightly different in latitude. It further substantiates the performance of the coupled model in simulating the actual LST pattern.

The investigation of hourly wind fields and corresponding rainfall evolution reveals an obvious and active diurnal phenomenon. Figure 10(a) presents the mean 850 hPa circulation pattern at 0600 LST (Local Standard Time) during the five-day period, which are overlaid by the associated lake-land breeze driven rainfall. The circulation pattern over the lake basin is characterized by the flow convergence over the northwestern sector of the lake where most of the rainfall occurred. The lake thus provided more water vapor along with the rising motion, which is related to the intriguing land breeze circulation, when the lake surface temperature is warmer than the adjacent land during the nighttime (Figure 10(b)). During the day, the thermal difference reverses and moves the cooler air inland, which gives rise to the divergence pattern in the lower troposphere over the lake. Nevertheless, such corresponding relation at 1500 LST is not quite evident here, although the model indeed captures divergence over the lake when the lake circulation is assumed to be fully developed. The simulated lake breeze circulation is relatively weaker than the land branch. Consequently, a significant amount of precipitation is produced over the lake region in the early morning with a land breeze dominating, while outside the lake surfaceand over the land in the afternoon. The simulated diurnal rainfall variability over four quadrants of the lake surface also verifies such land-lake breeze related features. The four quadrants are 1° × 1° square boxes (~10,000 km^2) over the lake surface and are designated as the northwest quadrant (NW: 0°-1°S, 32°-33°E), southwest quadrant (SW: 1°-2°S, 32°-33°E), northeast quadrant (NE: 0°-1°S, 33°-34°E), and southeast quadrant (SE: 1°-2°S, 33°-34°E) as in Anyah [5]. Three-hourly total rainfall data were used to derive diurnal cycles over each quadrant (Figure 11). The diurnal feature is noticeably illustrated and the diurnal cycle of rainfall is characterized by the nocturnal peak (midnight to early morning hours), and then rainfall intensity dramatically diminishes over the entire lake, thereafter, which is consistent with precious studies. The intense rainfall occurrence is concentrated over the western hemisphere. This is in accordance with the two-rainfall maxima pattern from observation, with the western and eastern sectors sharing similar features of the rainfall evolution at a 3-hour interval.

On the other hand, the cross-section of the vertical velocity along the two-rainfall maxima also confirmed the strong upward motion over the lake associated with land breeze circulation during nocturnal time. Figure 12 displays very strong ascending motion over the western sector of the lake, with maximum vertical velocity reaching 0.22 ms^{-1} and centering at 32.6°E, which coincides with the maximum rainfall at 0600 LST. The western branch of the upward motion extends from 850 hPa to the limited height and is associated with the deep convection, which can easily explain the significant rainfall over the western sector of the lake. Moreover, the upward motion over the eastern sector is not as strong as the western branch and the net subsidence mainly occupies near the lake surface. However, the entire lake surface is dominated by the descending motion at 1500 LST, while the ascending motion is primarily located over the surrounding land, which is related to the land rainfall. Such profiles are in accordance with the expected diurnal circulation and rainfall variability over the lake surface associated with the lake-land breeze circulation. When we look into the convergence/divergence pattern over the lake basin at the corresponding time, the characteristics are consistent with the diurnal feature captured from the vertical velocity flow pattern. There is strong convergence over the western sector of the lake early in the morning (Figure 13(a)), leading to intense upward motion along with the sufficient water vapor needed to bring about a significant amount of rainfall. The most active center of the convergence is located at around 850 hPa, which is in great agreement with the mean 850 hPa circulation pattern shown above. Conversely, the afternoon pattern (Figure 13(b)) shows weaker divergence over the lake basin, constraining at a relatively lower height and relatively strong convergence over the adjoining land.

Radar reflectivity diagnosed from the model output is very useful to present mesoscale fields and, thus, to

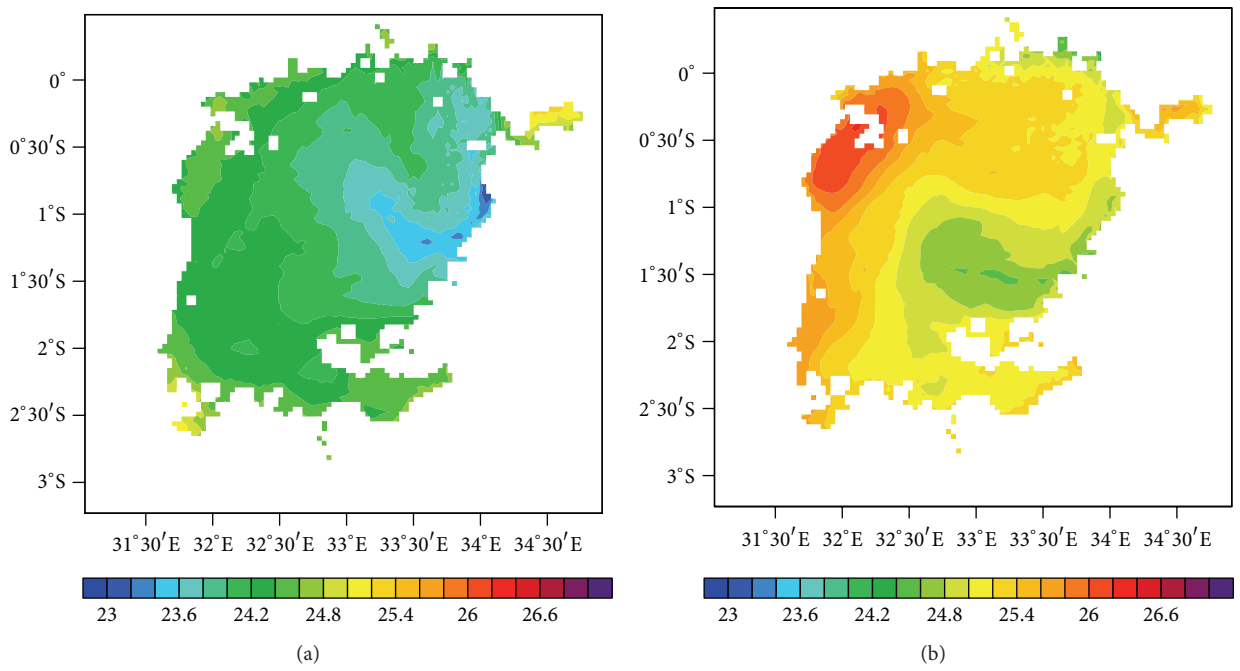

Figure 8: The lake surface temperature (in °C) after (a) 10 days and (b) two months of integration.

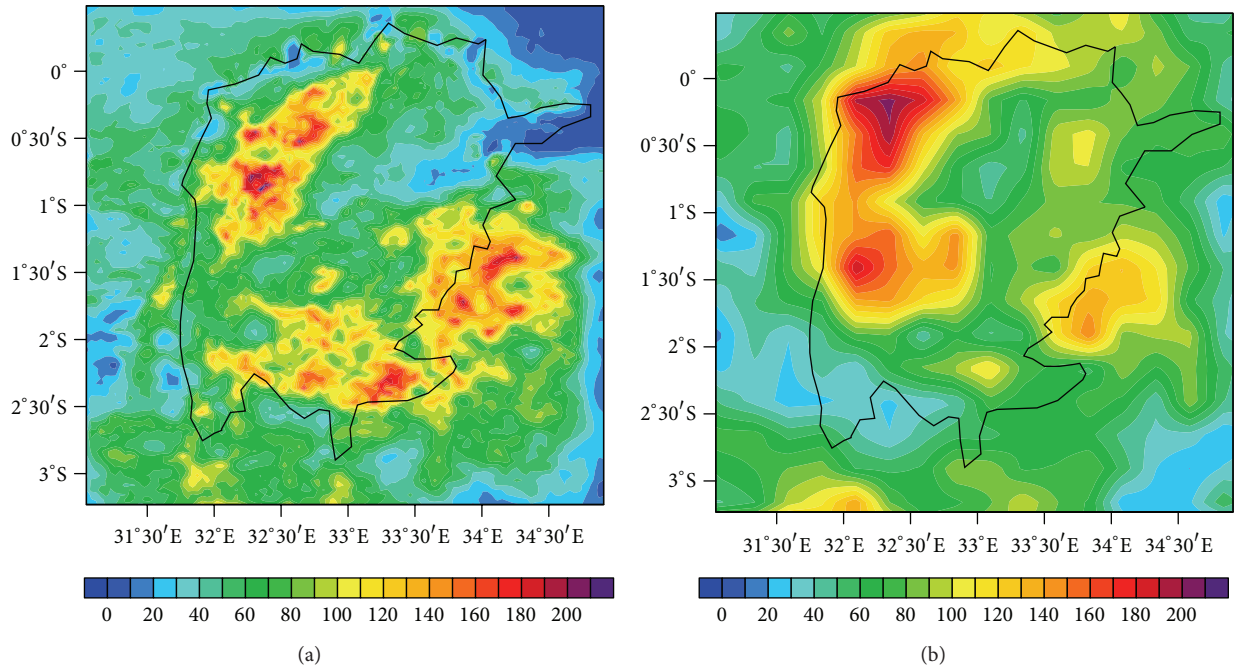

Figure 9: Total precipitation distribution from (a) the experiment with the lake surface temperature pattern from the coupled model and (b) the TRMM data.

help understand relevant mesoscale processes from high-resolution numerical models. The radar reflectivity used below is extracted and derived by a NCAR command language (NCL) function, which is computed from the simulated mixing ratios of grid-resolved hydrometeor species, assuming scattering by spherical particles of known constant density with an exponential size distribution [36]. Therefore, we tracked the radar reflectivity at a cross-section and observed a maximum radar reflectivity at a 3-hourly interval and obtained a pronounced relationship between lake precipitation and itself. Figure 14(a) shows strong radar reflectivity over the western sector of the lake, whose location is in great accordance with the maximum ascending motion and intense convergence zone. However, during the afternoon, it

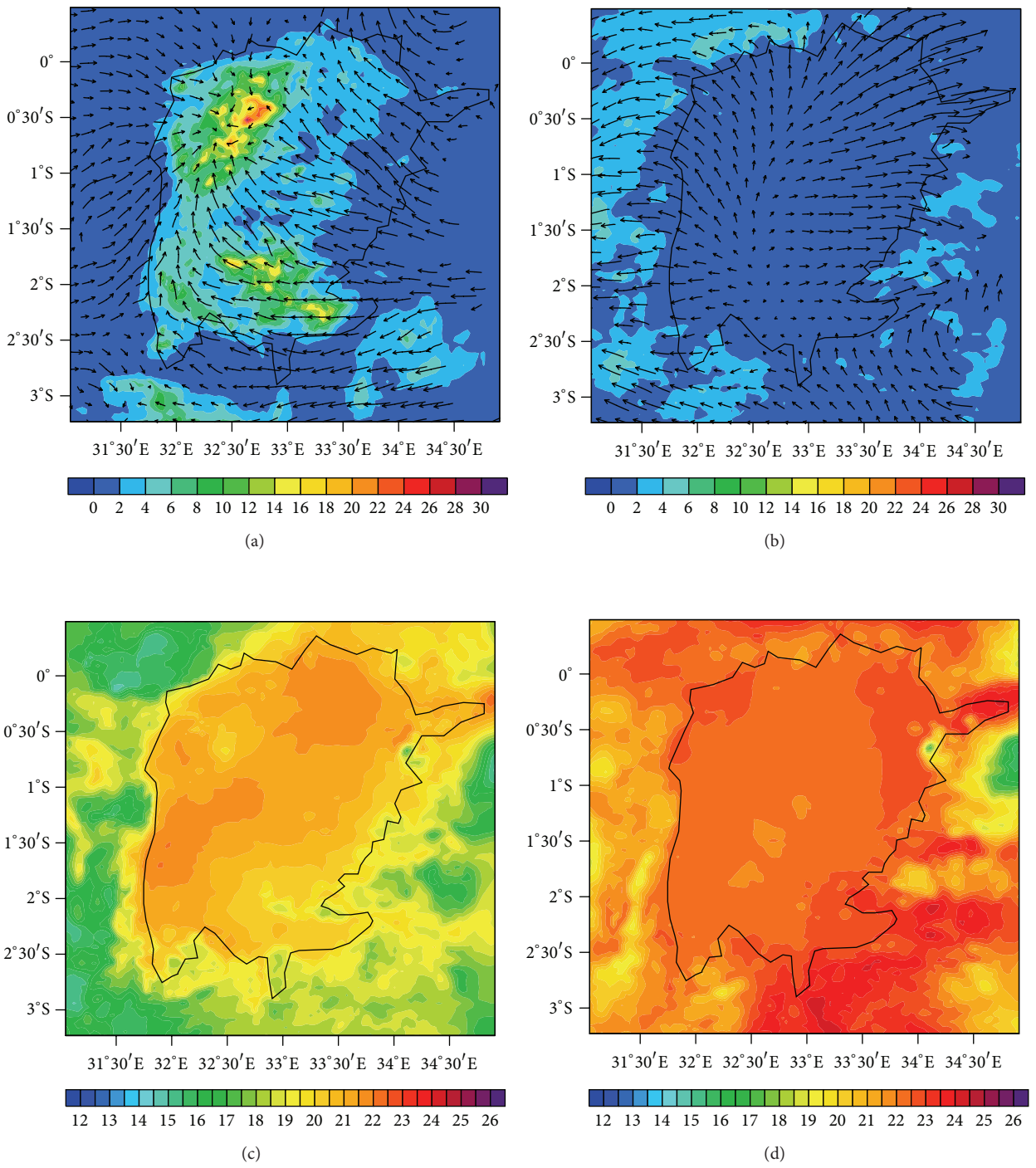

Figure 10: The 850 hPa mean flow (arrows) overlaid on precipitation (a, b) and the 2 m air temperature (c, d) over the LVB at 0600 LST (a, c) and 1500 LST (b, d).

appears that there are only negative values over the eastern lake region, which means only very tiny hydrometeors are detected. The result expectedly coincides with the fact that little precipitation occurred over the lake. When we look into the maximum radar reflectivity (Figure 15), its extent and concentrated location also serve as a mirror to the generated precipitation. The greater the intensity of maximum radar reflectivity, the larger the amount of rainfall over the lake and adjacent land area. In addition, it seems that the area of maximum radar reflectivity moves from east to west from the evolution of 3-hourly reflectivity. To allow for more direct viewing, the lake is divided into two parts between the equator and 2.25°S. Then, the time-longitude change of maximum radar reflectivity is computed for each part. The diurnal feature is more distinctly represented in this way. Figure 14 gives clear patterns of dominating westward propagation

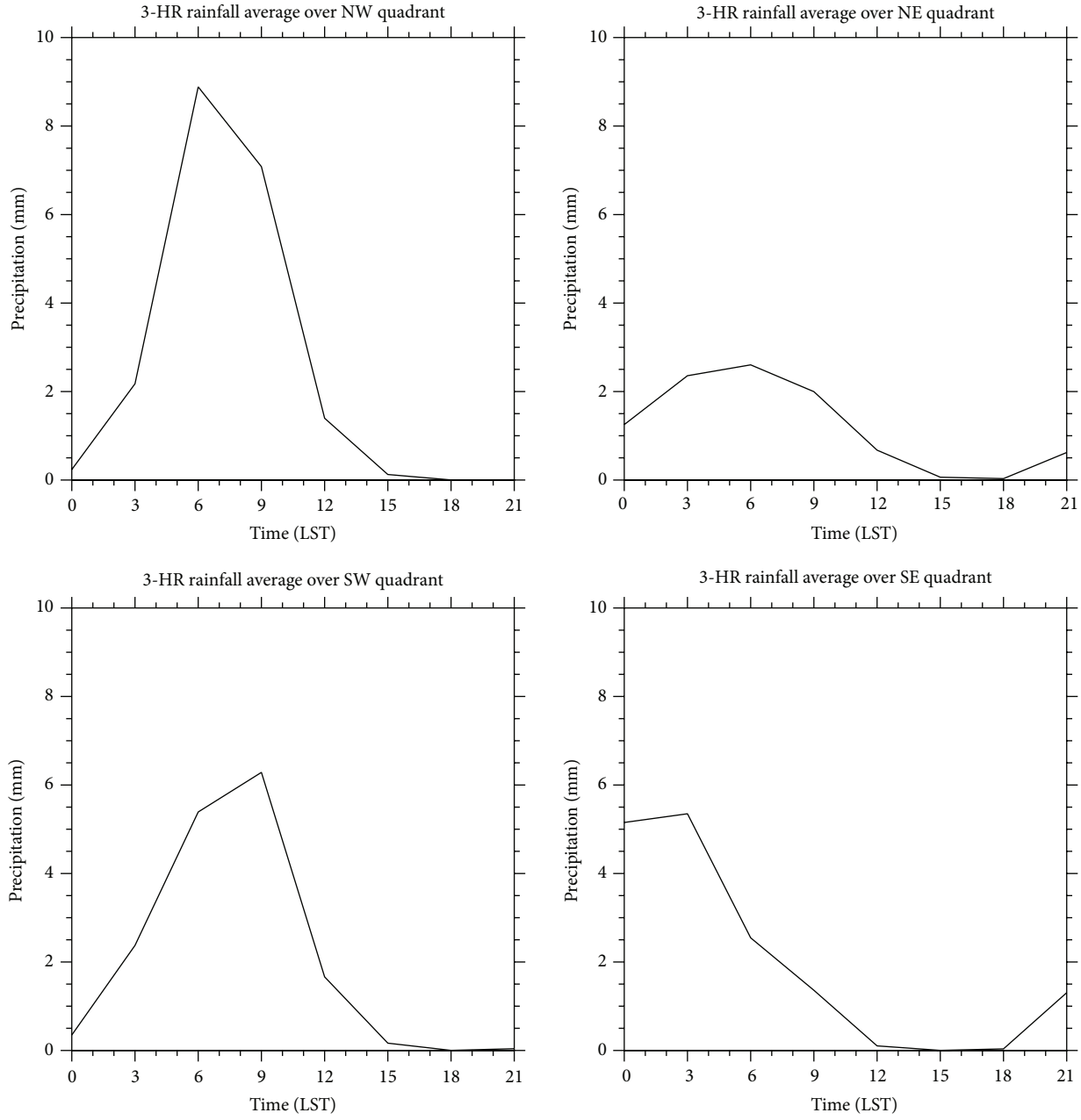

Figure 11: Time series of 3-hourly total rainfall over four quadrants of the lake.

over the entire lake. There are five apparent wavelengths over the simulated area and correspondingly, the period of wave motion is just one day, which in turn, fully verifies the diurnal characteristic of rainfall variability. Overall, the precipitation appears to be more intense and substantial over the lake during simulation period. The precipitation mainly occurs between midnight and the early morning hours (00-06 LST), which is representative of the nocturnal peak and is consistent with our foregoing discussions. Furthermore, the occurrence of domain precipitation is primarily centralized on the first day and the last two days and is shown over both parts of the lake. Nevertheless, there is an ever-present precipitation concentration over the eastern coast under the default setting and various lake surface temperature forcings. Since the simulation period falls into the short rainy season of Eastern Africa, we postulate that the southward progression of the ITCZ exerts a certain impact on such a persistent rainfall area.

4. Summary and Conclusions

Critical influence of lake surface temperature on the distribution of rainfall over Lake Victoria was demonstrated in a previous study. However, the current accessible datasets are lacking trustable gauge resources of variables over the lake. A coupled atmosphere-lake model was therefore introduced

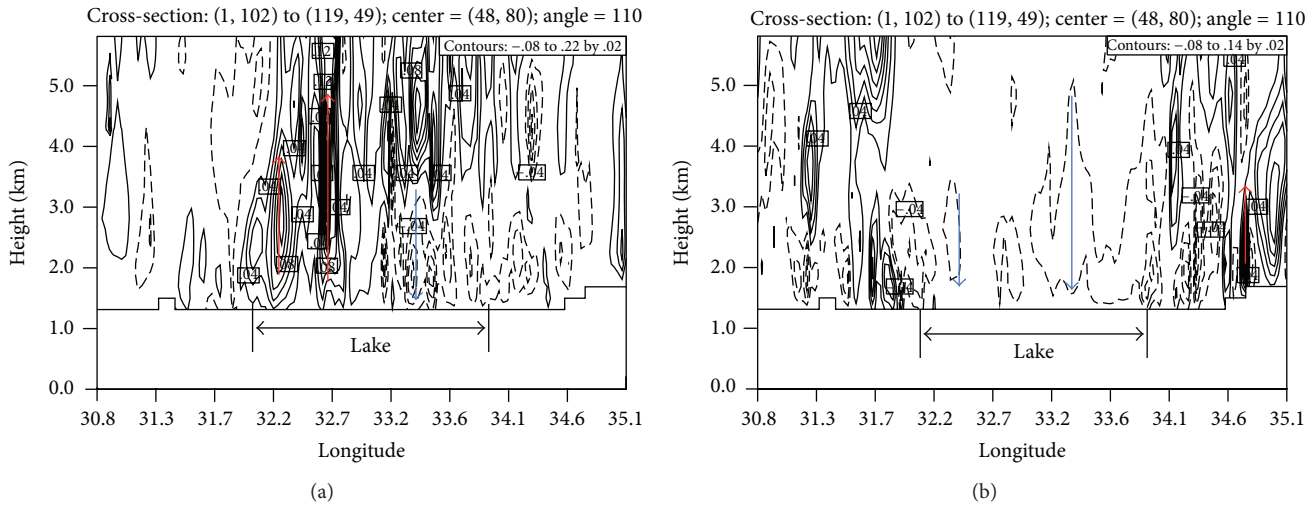

Figure 12: Cross-sections of vertical velocity at (a) 0600 LST and (b) 1500 LST along the two-rainfall maxima.

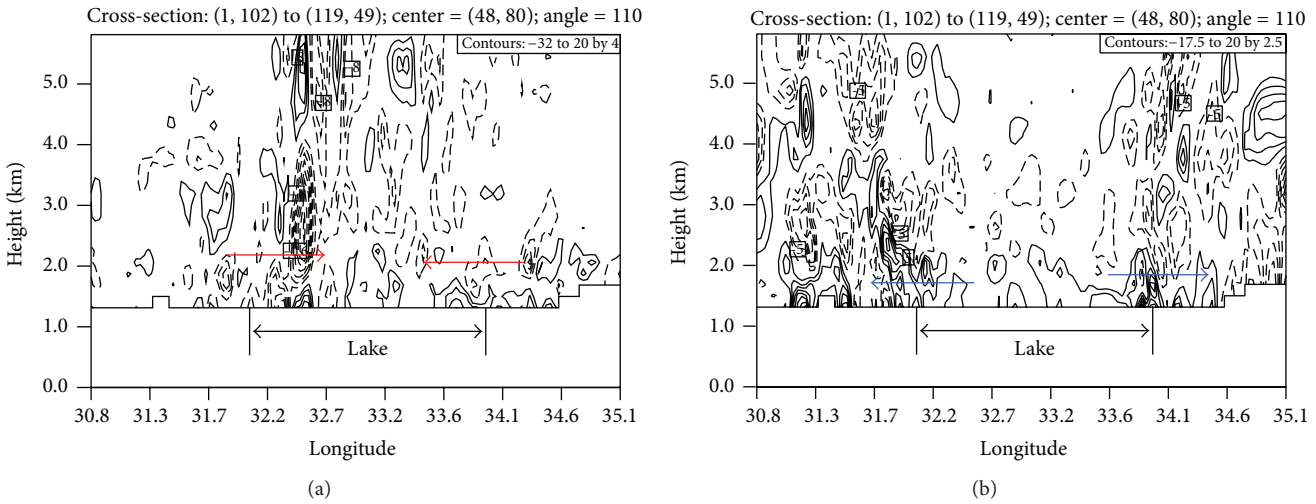

Figure 13: Cross-sections of divergence flow (10^{-5} m^{-1}) along the two-rainfall maxima at (a) 0600 LST and (b) 1500 LST.

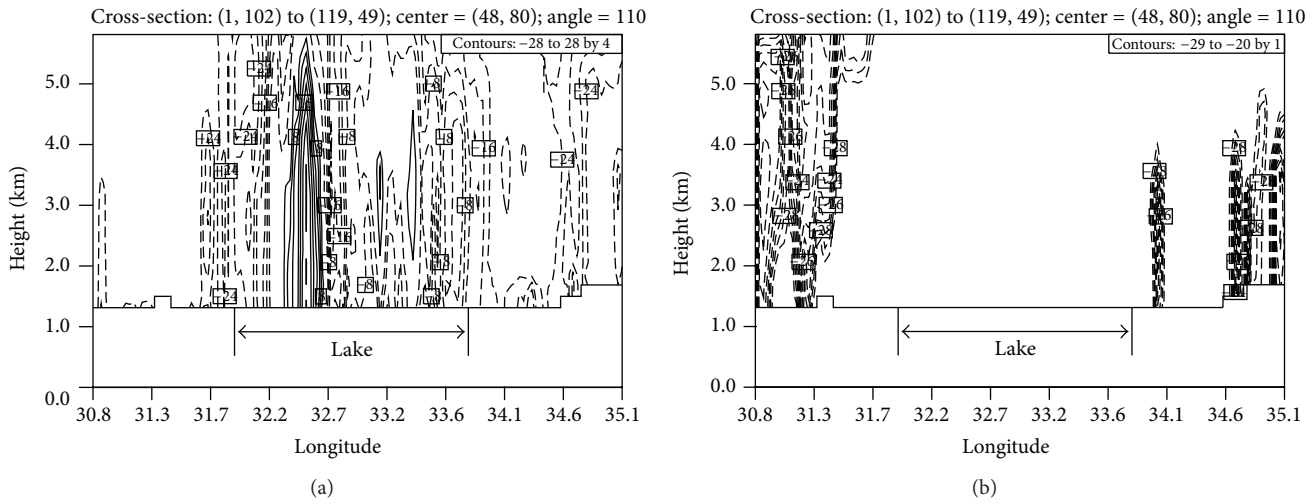

Figure 14: Cross-sections of radar reflectivity (in dBZ) along the two-rainfall maxima at (a) 0600 LST and (b) 1500 LST.

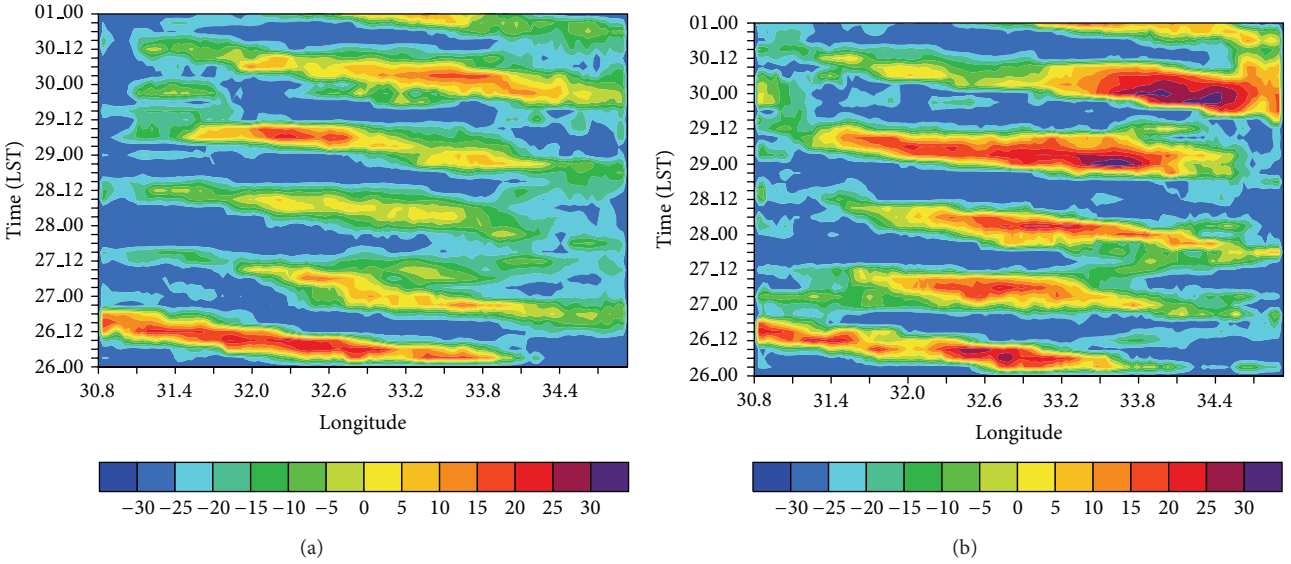

Figure 15: Time-longitude sections of maximum radar reflectivity (in dBZ) over (a) northern and (b) southern parts of the lake.

in order to produce realistic lake circulation, including its LST pattern, by taking into account air-lake interaction processes. The coupled atmosphere-lake model considers full exchange of time-dependent variables between atmosphere and lake in their interface and allows the mixings of energy in both vertical and horizontal directions in the lake. Results show that the produced LST pattern was characteristic of an eastward temperature gradient, as dictated by the lake bathymetry, with a shallower region over the western sector of the lake and a deeper area over the eastern part. The numerical simulation with a produced LST pattern obtained a better rainfall distribution compared with the observational data.

There was distinguished diurnal phenomenon detected during the succeeding examination and diagnostic analysis. The intense precipitation occurrence fell into the nocturnal peak between midnight and the early morning hours, which coincided with the strong land breeze circulation when the lake was warmer during the nighttime. However, the other branch was relatively weaker during the daytime and the lake was predominantly occupied by the descending motion, leading to divergence and less precipitation. It is consistent with the apparent features in vertical velocity and radar reflectivity patterns along rainfall maxima over the eastern and western lake hemispheres. In addition, the time-longitude analysis of the maximum radar reflectivity over both the northern and southern sections of the lake presented a remarkable westward propagation wave with a one-day period which, in turn, confirmed such diurnal features.

Besides, we selected ten physical schemes from cumulus, microphysical, and planetary boundary layer schemes to compare the total 36 possible combinations and obtain the optimal settings for the current short-term case. The primary findings were in great agreement with the previous studies that the MP and PBL appeared to exert relatively less influence than the Cu scheme on the simulated rainfall. The impacts of the domain size and lateral boundary conditions also showed their importance with domain center altering.

However, the real bathymetry data used in this study is crude and lacking other comparable variables, together resulting in insufficient and incomprehensive examination of the coupled simulations. The focus of this study is on the short-term rainfall over the lake region. The effect of atmosphere-lake interaction may take weeks and months to fully manifest itself. Therefore, short and long-term climatic simulations are needed to examine the effect and processes coupling the lake and the atmosphere over Lake Victoria in more depth and with greater certainty.

Conflict of Interests

The authors declare that there is no conflict of interests regarding the publication of this paper.

Acknowledgments

The authors are grateful to Ms. Katie Costa for the English proofreading. This study is supported by the National Science Foundation through Grant no. 553210.

References

[1] K. Bryan, S. Manabe, and R. C. Pacanowski, "A global oceanatmosphere climate model. Part II. The oceanic circulation," *Journal of Physical Oceanography*, vol. 5, pp. 30–46, 1975.

[2] S. Manabe and K. Bryan, "Climate calculations with a combined ocean-atmosphere model," *Journal of the Atmospheric Sciences*, vol. 26, pp. 786–789, 1969.

[3] S. Manabe, K. Bryan, and M. J. Spelman, "A global ocean-atmosphere climate model. Part I. The atmospheric circulation," *Journal of Physical Oceanography*, vol. 5, pp. 3–29, 1975.

[4] Y. Song, F. H. M. Semazzi, L. Xie, and L. J. Ogallo, "A coupled regional climate model for the Lake Victoria Basin of East Africa," *International Journal of Climatology*, vol. 24, no. 1, pp. 57–75, 2004.

[5] R. O. Anyah, *Modeling the variability of the climate system over Lake Victoria Basin [Ph.D. dissertation]*, North Carolina State University, 2006.

[6] W. Thiery, A. Martynov, F. Darchambeau et al., "Understanding the performance of the FLake model over two African Great Lakes," *Geoscientific Model Development*, vol. 7, pp. 317–337, 2014.

[7] W. Thiery, "LakeMIP Kivu: evaluating the representation of a large, deep tropical lake by a set of one-dimensional lake models," *Tellus A*, vol. 66, Article ID 21390, 2014.

[8] L. Xie, B. Liu, H. Liu, and C. Guan, "Numerical simulation of tropical cyclone intensity using an air–sea–wave coupled prediction system," *Advanced Geosciences*, vol. 18, pp. 19–43, 2010.

[9] B. Liu, H. Liu, L. Xie, C. Guan, and D. Zhao, "A Coupled atmosphere-wave-ocean modeling system: simulation of the intensity of an idealized tropical cyclone," *Monthly Weather Review*, vol. 139, no. 1, pp. 132–152, 2011.

[10] H. Liu, B. L. Liu, L. Xie, and K. Zhang, "Simulation of ocean responses to an idealized landfalling tropical cyclone using a coupled atmosphere-wave-ocean modeling system," *Tropical Cyclone Research and Review*, vol. 1, no. 3, pp. 373–389, 2012.

[11] X. Sun, L. Xie, F. H. M. Semazzi, and B. Liu, "Effect of lake surface temperature on the spatial distribution and intensity of the precipitation over Lake Victoria Basin," Monthly Weather Review, In reviews.

[12] W. C. Skamarock, J. B. Klemp, J. Dudhia et al., "A description of the advanced research WRF version 2," NCAR Tech. Note NCAR/TN-4681STR, 2007.

[13] G. L. Mellor and A. F. Blumberg, "Modeling vertical and horizontal diffusivities with the sigma coordinate system," *Monthly Weather Review*, vol. 113, pp. 1380–1383, 1985.

[14] R. Jacob, J. Larson, and E. Ong, "M—×—N communication and parallel interpolation in community climate system model version 3 using the model coupling toolkit," *International Journal of High Performance Computing Applications*, vol. 19, no. 3, pp. 293–307, 2005.

[15] J. Larson, R. Jacob, and E. Ong, "The model coupling toolkit: a new Fortran90 toolkit for building multiphysics parallel coupled models," *International Journal of High Performance Computing Applications*, vol. 19, no. 3, pp. 277–292, 2005.

[16] A. P. Craig, R. Jacob, B. Kauffman et al., "Cpl6: The new extensible, high performance parallel coupler for the community climate system model," *International Journal of High Performance Computing Applications*, vol. 19, no. 3, pp. 309–328, 2005.

[17] J. C. Warner, C. R. Sherwood, R. P. Signell, C. K. Harris, and H. G. Arango, "Development of a three-dimensional, regional, coupled wave, current, and sediment-transport model," *Computers and Geosciences*, vol. 34, no. 10, pp. 1284–1306, 2008.

[18] W. P. O'Connor and D. J. Schwab, "Sensitivity of great lakes forecasting system nowcasts to meteorological fields and model parameters," in *Proceedings of the 3rd International Conference on Estaurine and Coastal Modeling*, M. L. Spaulding, K. Bedford, A. Blumberg, R. Cheng, and C. Swanson, Eds., pp. 149–157, American Society of Civil Engineers, Oak Brook, Ill, USA, 1994.

[19] X. Yin and S. E. Nicholson, "The water balance of Lake Victoria," *Hydrological Sciences Journal*, vol. 43, no. 5, pp. 789–812, 1998.

[20] NOAA, "National Oceanic and Atmospheric Administration Changes to the NCEP Meso Eta Analysis and Forecast System: increase in resolution, new cloud microphysics, modified precipitation assimilation, modified 3DVAR analysis," 2001.

[21] G. A. Grell and D. Dévényi, "A generalized approach to parameterizing convection combining ensemble and data assimilation techniques," *Geophysical Research Letters*, vol. 29, no. 14, pp. 38-1–38-4, 2002.

[22] J. E. Pleim, "A combined local and nonlocal closure model for the atmospheric boundary layer. Part I. Model description and testing," *Journal of Applied Meteorology and Climatology*, vol. 46, no. 9, pp. 1383–1395, 2007.

[23] J. E. Pleim, "A combined local and nonlocal closure model for the atmospheric boundary layer. Part II: application and evaluation in a mesoscale meteorological model," *Journal of Applied Meteorology and Climatology*, vol. 46, no. 9, pp. 1396–1409, 2007.

[24] A. C. M. Beljaars, "The parametrization of surface fluxes in large-scale models under free convection," *Quarterly Journal—Royal Meteorological Society*, vol. 121, no. 522, pp. 255–270, 1995.

[25] F. Chen and J. Dudhia, "Coupling and advanced land surface-hydrology model with the Penn State-NCAR MM5 modeling system. Part I: Model implementation and sensitivity," *Monthly Weather Review*, vol. 129, no. 4, pp. 569–585, 2001.

[26] J. Crétat, B. Pohl, Y. Richard, and P. Drobinski, "Uncertainties in simulating regional climate of Southern Africa: sensitivity to physical parameterizations using WRF," *Climate Dynamics*, vol. 38, no. 3-4, pp. 613–634, 2012.

[27] B. Pohl, J. Crétat, and P. Camberlin, "Testing WRF capability in simulating the atmospheric water cycle over Equatorial East Africa," *Climate Dynamics*, vol. 37, no. 7-8, pp. 1357–1379, 2011.

[28] N. Davis, J. Bowden, F. Semazzi, L. Xie, and B. Önol, "Customization of RegCM3 regional climate model for eastern Africa and a tropical Indian Ocean domain," *Journal of Climate*, vol. 22, no. 13, pp. 3595–3616, 2009.

[29] A. Dai, "Precipitation characteristics in eighteen coupled climate models," *Journal of Climate*, vol. 19, no. 18, pp. 4605–4630, 2006.

[30] L. R. Leung, Y. Qian, X. Bian, W. M. Washington, J. Han, and J. O. Roads, "Mid-century ensemble regional climate change scenarios for the western United States," *Climatic Change*, vol. 62, no. 1–3, pp. 75–113, 2004.

[31] A. Arakawa, "The cumulus parameterization problem: past, present, and future," *Journal of Climate*, vol. 17, pp. 2493–2525, 2004.

[32] A. Arakawa and W. Schubert, "Interaction of a cumulus cloud ensemble with the large-scale environment, part I," *Journal of the Atmospheric Sciences*, vol. 31, pp. 674–701, 1974.

[33] J. Dudhia, "Numerical study of convection observed during the winter monsoon experiment using a mesoscale two-dimensional model," *Journal of the Atmospheric Sciences*, vol. 46, no. 20, pp. 3077–3107, 1989.

[34] E. J. Mlawer, S. J. Taubman, P. D. Brown, M. J. Iacono, and S. A. Clough, "Radiative transfer for inhomogeneous atmospheres: RRTM, a validated correlated-k model for the longwave," *Journal of Geophysical Research*, vol. 102, no. 14, pp. 16663–16682, 1997.

[35] M. A. Friedl, D. K. McIver, J. C. F. Hodges et al., "Global land cover mapping from MODIS: algorithms and early results," *Remote Sensing of Environment*, vol. 83, no. 1-2, pp. 287–302, 2002.

[36] M. T. Stoelinga, "Simulated equivalent reflectivity factor as currently formulated in RIP: description and possible improvements," Technical Report, 2005, http://www.atmos.washington.edu/~stoeling/RIP_sim_ref.pdf.

[37] S. H. Chen and W. Y. Sun, "A one-dimensional time dependent cloud model," *Journal of the Meteorological Society of Japan*, vol. 80, no. 1, pp. 99–118, 2002.